Suyehiro, K., Sacks, I.S., Acton, G.D., and Oda, M. (Eds.)
Proceedings of the Ocean Drilling Program, Scientific Results Volume 186

14. Fluid Geochemistry in the Japan Trench Forearc (ODP Leg 186): A Synthesis[1]

Achim Kopf,[2] Germán Mora,[3] Annette Deyhle,[2] Shaun Frape,[4] and Reinhard Hesse[5]

ABSTRACT

We report results from shipboard analyses and postcruise studies on gas and interstitial pore waters from Ocean Drilling Program (ODP) Sites 1150 and 1151, both penetrating ~1200 m of subseafloor sediment from the upper Japan Trench forearc. Apart from concentrations of hydrocarbons in the gas phase, pore waters were analyzed for various element concentrations and stable isotopic composition of Cl and B.

Both drill sites are characterized by two opposing trends in the downhole element profiles in the pore waters. A strong depletion of Na, K, Cl, and salinity is contrasted by an equally profound increase in specific mobile elements such B, Li, or Sr with depth. For example, although chlorinity drops to about one-half the seawater (SW) value, the same fluid shows a ~10-fold enrichment of boron and ~40-fold increase in Li (relative to SW). The strong variations in concentration occur in the deep, tectonically deformed part of the two drill sites, which show abundant fractures and two shear zones (the latter at Site 1150). The heavily fractured portions are further characterized by low $\delta^{37}Cl$ values (down to –1.1‰) and high $\delta^{11}B$ values (~40‰–46‰). In the gas phase, the fractured intervals show significant increases in hydrocarbon contents and C_1/C_2 ratios. The profound excursions in gas and water profiles can be best explained by deep-seated processes. These may include clay mineral diagenesis, alteration of tephra from the Japan and Izu arcs, transformation of biogenic silica from abundant diatoms, and maturation of organic matter. The strong enrichment of some mobile elements (e.g., Sr, B, and Li) attests that enhanced fluid flow through

[1]Kopf, A., Mora, G., Deyhle, A., Frape, S., and Hesse, R., 2003. Fluid geochemistry in the Japan Trench forearc (ODP Leg 186): a synthesis. *In* Suyehiro, K., Sacks, I.S., Acton, G.D., and Oda, M. (Eds.), *Proc. ODP, Sci. Results,* 186, 1–23 [Online]. Available from World Wide Web: <http://www-odp.tamu.edu/publications/186_SR/VOLUME/CHAPTERS/117.PDF>. [Cited YYYY-MM-DD]
[2]Scripps Institution of Oceanography, University of California, San Diego, 9500 Gilman Drive, La Jolla CA 92093-0244, USA. Correspondence author: **akopf@ucsd.edu**
[3]Department of Geology and Atmospheric Sciences, Iowa State University, Ames IA 50011-3212, USA.
[4]Department of Earth Sciences, University of Waterloo, Waterloo ON N2L 3G1, Canada.
[5]Institut für Geologie, Mineralogie, und Geophysik, Ruhr-Universität Bochum, Universitätsstrasse 150, 44801 Bochum, Germany.

Initial receipt: 18 June 2002
Acceptance: 6 March 2003
Web publication: 1 July 2003
Ms 186SR-117

permeable shear zones in the Japan Trench forearc (most prominently at Site 1150) may be an efficient mechanism to return those elements from the deep forearc back into the ocean.

INTRODUCTION

Recently, Ocean Drilling Program (ODP) Leg 186 drilling (Sacks, Suyehiro, Acton, et al., 2000) targeted the Japan Trench forearc offshore Honshu Island, where ~130-m.y.-old Pacific plate oceanic lithosphere is subducted beneath Eurasia. Previous geophysical investigation (e.g., Nasu et al., 1980; von Huene and Culotta, 1989) and scientific drilling (Deep Sea Drilling Project [DSDP] Legs 56, 57, 87; Scientific Party, 1980a, 1980b; Kagami, Karig, Coulbourn, et al., 1986) documented a history of complex tectonic forearc dynamics. Whereas little accretion has occurred during the Neogene, erosion related to subduction has caused subsidence of the continental margin off northern Japan (von Huene and Lallemand, 1990). Two holes, at Sites 1150 and 1151, were drilled into the seismic and aseismic portion of the forearc with the main purpose of installing downhole instruments. However, the ~1200 m of sediment recovered from each of these holes also revealed some interesting details concerning deformation and deep-seated fluid flow of the area. Here, we report geochemical results from both headspace gas and interstitial water samples from the two sites to characterize fluid flow and sediment-water interaction in the partly tectonized material. Shipboard data are complemented by postcruise research of element concentrations and isotopic signatures in the waters (e.g., Deyhle and Kopf, 2002). The objectives of this summary paper are to combine all geochemical evidence and relate it to different diagenetic processes operating at depth, such as opal-A/opal-CT/quartz reactions, clay mineral transformation, adsorption/desorption reactions, and alteration of ash and tephra.

GEOLOGICAL SETTING

The Japan Trench parallels the roughly north-south–striking volcanic arc of northern Honshu Island, where Pacific oceanic basement is consumed beneath the Eurasian plate at a convergence rate of ~9 cm/yr (von Huene et al., 1982). The area has experienced abundant microseismic events as well as several $M > 7$ earthquakes in historic time (Suyehiro and Nishizawa, 1994; Sacks, Suyehiro, Acton, et al., 2000). The bulk of the forearc is composed of Cretaceous accreted strata (based on moderate *P*-wave velocity and landward-dipping reflectors) (see von Huene et al., 1994) discordantly overlain by thick forearc basin fills and thinner slope apron sediments. The absence of young accreted strata in the forearc as well as multichannel seismic records (Scientific Party, 1980b) attest that most of the sediment entering the trench is subsequently subducted. Earlier drilling campaigns (DSDP Legs 56, 57, and 87; Scientific Party, 1980a, 1980b; Kagami, Karig, Coulbourn et al., 1986) provided evidence for subsidence of ~6 km, resulting from basal erosion of the continental slope and forearc wedge, which also caused the trench to retreat an estimated 50–75 km (Langseth et al., 1981; von Huene and Lallemand, 1990). At present, the forearc morphology is characterized by a steep and rugged inner trench slope, which is overlain by a deep-sea terrace and a 600-km-wide forearc basin (Cadet et al.,

1985). Both Sites 1150 and 1151 were drilled into the forearc basin fill, but neither hole reaches the Cretaceous.

DRILLING RESULTS FROM ODP LEG 186

During ODP Leg 186 (Sacks, Suyehiro, Acton, et al., 2000), ~1200 m of sediment was penetrated at Site 1150 in a seismically active portion of the Japan Trench forearc. The sedimentary section drilled recovered dominantly hemipelagic diatomaceous silty clays and claystones of late Miocene to Holocene age (0–9.9 Ma). Cores from 0 to 420 m below seafloor (mbsf) are soft diatomaceous silty clay of Pliocene–Quaternary age with interbeds rich in ash layers, biogenic opal-A, or dolomite (Fig. F1A) (Sacks, Suyehiro, Acton, et al., 2000). From 420 to 650 mbsf, similar but more consolidated lithologies of latest Miocene age were recovered. Below ~650 mbsf, cores consist mainly of well-lithified diatomaceous claystone of late Miocene age (Fig. F1A). Prominent ash and tephra layers are present at the top and base of the hole, with a notable increase in volcanic deposits (>10 vol% of total sediment) between 0.5 and ~3 Ma (Fig. F1A) (Sacks, Suyehiro, Acton, et al., 2000). Coarser-grained turbiditic deposits are found between 650 and 800 mbsf. Intervals rich in opal-A (and opal-CT) are found throughout the hole (even at ~1050–1118 mbsf), with scanning electron microscopy (SEM) evidence for largely intact diatom tests (S. Saito, pers. comm., 2001). The resistance of diatoms to collapse causes the anomalously high average porosities of >50% at depths exceeding 1000 mbsf (Sacks, Suyehiro, Acton, et al., 2000). Sediment accumulation was low from ~0.5 to 3 Ma but reaches maxima between 6 and 8 Ma (up to 220 m/m.y.) (Fig. F1A) (Sacks, Suyehiro, Acton, et al., 2000). The average sedimentation rate is 119 m/m.y. Faulting and brittle fractures are abundant from below 700 mbsf to the base of the hole, with two shear zones at 900–950 and 1030–1070 mbsf.

At Site 1151, the sedimentary sequence ranges from Holocene to middle Miocene age (0–16.3 Ma) (Fig. F1B), showing clayey diatom ooze and diatomaceous silty clay to claystone as major lithologies. Clays are soft in the upper 350 mbsf, firm between 350 and 650 mbsf, and well consolidated below (Fig. F1B) (Sacks, Suyehiro, Acton, et al., 2000). Intercalations of volcaniclastic ash, pumice, silt and sand, and opal-rich diatom layers are present over wide portions of the section. Ash is most abundant in sediments of 0.5- and ~4-Ma age. Brittle deformation structures dominate below 400 mbsf but are less pervasive than at Site 1150. Numerous fractures and microfaults observed in the core and logging data are consistent with either the general east-west extensional stress field corresponding to the opening of the Japan Sea or the current east-west compressional tectonic stress field across the Japan Trench forearc. The average sedimentation rate at Site 1151 is only 24 m/m.y. for Site 1151 but shows a wide variation from <10 to 180 m/m.y. (Sacks, Suyehiro, Acton, et al., 2000).

At both sites, the high remaining porosities together with the fractures have profound effects on the fluid chemistry, as they provide permeable pathways. Elevated porosities may be attributed to the—at least temporarily—high sedimentation rates into the forearc basin; however, recent triaxial consolidation tests confirm that the formation is not overpressured (M. Ask, pers. comm., 2001). The reason for elevated porosity at depth may be a combination of the unaltered, intact diatom tests as well as a secondary porosity resulting from brittle failure in the deeper part of the succession. At Site 1150, faulting and brittle fractures

F1. Simplified drilling information, p. 17.

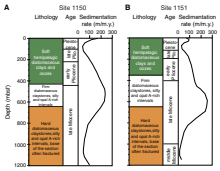

(i.e., secondary porosity) are complemented by two shear zones at 900–950 and 1030–1070 mbsf. The geothermal gradient in the Leg 186 area was estimated from temperature measurements to range around 29°–36°C/km (Sacks, Suyehiro, Acton, et al., 2000).

METHODS

Totals of 39 (Site 1150) and 29 (Site 1151) fluid samples were analyzed for alkalinity, salinity, and concentrations of Cl, Ca, Mg, K, Na, Li, and Sr. All these analyses were carried out on board the *JOIDES Resolution* during ODP Leg 186. Analytical procedures were outlined in the "Explanatory Notes" chapter in the Leg 186 *Initial Reports* volume (Shipboard Scientific Party, 2000) and will not be repeated here. Boron concentrations of the pore waters were determined by inductively coupled plasma–atomic emission spectrometer (ICP-AES; Jobin-Yvon 170 Ultrace) and by inductively coupled plasma–mass spectrometer (ICP-MS; VG-Plasmaquad PQ1) at Kiel University (Germany). Boron isotope measurements were carried out using a Finnigan MAT 262 negative thermal ionization mass spectrometer at GEOMAR, Kiel (Germany). The BO_2^- ion method was used in measurement of boron isotope ratios, following the procedure outlined in Zuleger and Erzinger (1991). Internal precision is typically ±0.05‰ (2 σ_{mean}) on average; external reproducibility is ±0.5‰.

In addition to the analyses on all the interstitial water samples recovered during ODP Leg 186, $\delta^{37}Cl$ isotope measurements were carried out on 19 selected fluid samples from Site 1150. Analyses were conducted at the University of Waterloo (Canada) using a VG SIRA 9 mass spectrometer. The method measures CH_3Cl in an adaptation of procedures developed by Kaufmann (1984), as is detailed in Sie and Frape (2002). Measurements were made with a precision of ±0.15‰ (1 σ) based on repeat analyses of standard mean ocean chloride (SMOC).

After the standard headspace sampling of the cores (following Kvenvolden and McDonald, 1986), gas samples were analyzed on board the *JOIDES Resolution* using a HP6890 gas chromatograph (Sacks, Suyehiro, Acton, et al., 2000). Free-gas samples were also analyzed with a natural gas analyzer attached to the HP6890, where two different columns are used for detection (for details, refer to Shipboard Scientific Party, 2000). Light hydrocarbon concentrations are reported in parts per million (ppm; after calibration to authentic standards) and as C_1/C_2 ratios.

RESULTS

Element Concentrations in Pore Waters

Site 1150

In Site 1150 pore waters, an overall decrease in salinity and Cl content is observed with depth. Chlorinity drops from seawater values near the top of the succession (~550 mM) to values near 300 mM at the base of the hole (Fig. F2A). Similarly, salinity drops from 34 mM at the top to ~18 mM near the base of the hole (Fig. F2B). However, this freshening does not occur continuously but is less pronounced in the upper 550 m of the drill hole. Farther below, where faulting and abundant fractures have created elevated secondary porosity of the claystones, Cl drops

F2. Pore water concentrations, Site 1150, p. 18.

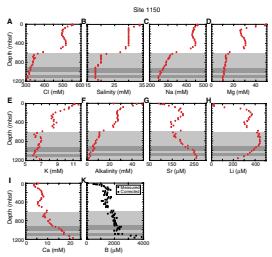

from ~480 mM (~510 mbsf) to 390 mM (~590 mbsf) and further to ~340 mM (~620 mbsf) (see Fig. F2A). Coincidently, downhole profiles of Na (Fig. F2C), Mg (Fig. F2D), and K (Fig. F2E) closely resemble those of Cl. The curves are nevertheless not identical, so simple dilution patterns can not explain the variation. A very similar curve is seen for the alkalinity, which—apart from a drastic increase from 24 mM (~20 mbsf) and 49 mM (~40 mbsf)—decreases continuously downhole to ~2 mM at the base of the hole (Fig. F2F). The correlation between abundant fractures (shaded intervals in Fig. F2) and low chlorinity suggests an influence of deep-seated fluids possibly originating from clay mineral dehydration reactions (Fitts and Brown, 1999) or alteration of biogenic silica (Kastner, 1981; see discussion below).

Sr concentrations show an overall increase with depth, which is characterized by two prominent excursions (Fig. F2G). The first interval of Sr enrichment is between ~50 and 350 mbsf, which corresponds to a period where volcanic activity and tephra deposition were most abundant in the area (Fig. F1B) (Sacks, Suyehiro, Acton, et al., 2000). The second interval where Sr enrichment is even more profound is observed at the base of the hole (~1000–1200 mbsf, where Sr ranges around 240–260 µM) (see Fig. F2G). Here again, the Sr excursion seems to correspond to a Miocene maximum in volcanic activity (see Fig. F1). As it has been pointed out earlier, both ash alteration (e.g., Hawkesworth and Elderfield, 1978) and calcite recrystallization (Sayles and Manheim, 1975) may account for such Sr release to the pore fluid (see discussion below). Li concentrations resemble the Sr trend in the upper part of the hole, where values rise from seawater (SW) concentration to ~360 µM (Fig. F2H). The overall enrichment relative to SW, however, is much more profound for Li than it is for Sr. In the fractured interval, however, Li initially increases (up to ~440 µM, or ~40-fold SW) but then drops to ~240 µM in the deepest pore water samples (Fig. F2H). This depletion in the Miocene succession may either be due to Li uptake into the sediment or could be explained by freshening. Unlike lithium, Ca shows a bimodal increase with depth, the first maximum between 200 and 300 mbsf (Fig. F2I, which coincides with almost every other element studied) and the second, more profound peak at the base of the hole. Here, Ca contents climb to >5-fold SW concentration, with a maximum of >21 mM (Fig. F2I). The Ca trend shows a commensurate behavior with Mg (Fig. F2D), which reflects uptake of Mg from seawater into the sediment during diagenetic processes (see below).

Boron concentrations (Fig. F2K), which have been corrected based on temperature, porosity, and pH following the method detailed in You et al. (1996), also show a strong enrichment relative to SW. B contents of pore waters from the subsurface sediments are generally slightly higher than seawater (420 µM) (see Fig. F2K). This phenomenon has been observed previously and can be interpreted as a result of bacterial degradation of organic matter and accompanying B release into the fluid (e.g., Harder, 1973; You et al., 1993, 1995). Apart from these data, B at Site 1150 increases consistently to ~1100–1500 µM (i.e., 3- to 4-fold seawater) at 500–550 mbsf (Fig. F2K). Below 600 mbsf, a considerable shift to much higher B contents of ~1700–2200 µM occurs. At the very base of the hole, a pronounced B maximum of up to 9.3-fold seawater concentration exists (3600–3900 µM). Our results imply that boron is removed from the solid phase (possibly from both clays and, to a lesser extent, volcanic ash) in considerable amounts, with the B removal from the solids and subsequent enrichment in the pore waters being more

obvious in the firm and hard parts of the sedimentary succession (see "Discussion," p. 8).

Site 1151

Pore water profiles at Site 1151 show fewer similarities between the various constituents than do those from Site 1150 (Fig. F2). Both chlorinity (Fig. F3A) and salinity (Fig. F3B) show a more or less continuous decrease with depth. Chlorinity almost immediately drops from near SW values (550 mM) to ~500 mM (~100–280 mbsf) (Fig. F3A), before a linear decrease causes freshening to values of ~300 mM at the base of the hole. Salinity mirrors this trend, with a decrease from 34 mM near the seafloor to about one-half this concentration at ~1100 mbsf (~18 mM) (Fig. F3B). Sodium contents (Fig. F3C) as well as magnesium contents (Fig. F3D) closely resemble those of chlorine. The continuous downhole decrease is best explained by pore water freshening processes, either in situ or at depth (see discussion below). This also applies to the potassium curve (Fig. F3E), where K concentrations drop to one-half their initial value at the base of the sedimentary succession.

However, other element trends show peculiar excursions dissimilar from the linear decrease observed for chlorinity, salinity, Na, Mg, and K. Most notably, alkalinity reaches a maximum at ~200 mbsf and an increase to ~24 mM at ~400 mbsf (Fig. F3F) and then decreases steadily over the fractured interval to values <3 mM at the base of the hole. By contrast, Sr content shows an initial increase to ~120 µM (SW = ~80 µM) but drops back to ~100 µM at 600 mbsf (Fig. F3G). From this depth, which in broad terms corresponds to the onset of induration of the clays and brittle failure and fracture development, a profound increase to >230 µM (~3-fold SW) is observed. Lithium shows an even more enigmatic trend, which again is dissimilar from Sr and alkalinity but also from the earlier profiles (Figs. F3A–E). After a strong linear increase from SW concentration to ~460 µM at ~700 mbsf (Fig. F3H), values stay at this high level in the 200-m interval below but then decrease from 900 mbsf toward the base of the hole. After the significant enrichment to >40-fold SW value, Li is only ~270 µM in the lowermost part of the succession (Fig. F3H). Ca contents show a negative relationship with Mg with the upper half of the sedimentary succession, having an almost constant Ca content of ~4 mM in the pore water, whereas a strong linear increase dominates the lower half (600–1100 mbsf) (Fig. F3I). Maximum concentrations exceed 18 mM, which represents a 4.5-fold enrichment relative to seawater.

Concentration of B increases at a relative continuous rate with depth at Site 1151 (Fig. F3K). The uppermost 600 mbsf is characterized by a gentle enrichment, reaching ~2-fold seawater B concentration at 400 mbsf (800 mM) and ~3-fold SW concentration (~1200 mM) at 600 mbsf. Below 600 mbsf, the B increase is steeper toward maximum concentrations of 2800 µM (i.e., 7-fold SW) but does not reach B contents at Site 1150 (~9.3-fold SW).

F3. Pore water concentrations, Site 1151, p. 19.

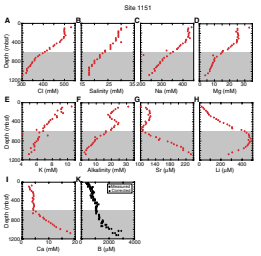

Isotope Results from Pore Waters

Site 1150

Values of $\delta^{37}Cl$ show an overall decrease with depth (Fig. F4). Compared to seawater (0‰), negative values occur from 25 mbsf downward, with a sharp decrease around 550 mbsf. Similar to Cl concentrations,

F4. Cl isotopes, p. 20.

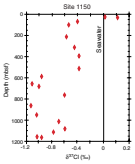

this excursion seems to be linked to fractured claystones, which allow deeper fluids to migrate upward. The most negative values, approximately –1.1‰, are observed near the upper of the two shear zones (930–970 mbsf), supporting the notion that some of these fluids are derived from depth. Compared to other convergent margins (e.g., Nankai farther southwest, where $\delta^{37}Cl$ drops to –7.8‰) (Kastner and Spivack, 2001), the negative shift of the $\delta^{37}Cl$ data with depth is less pronounced in the Japan Trench, whereas the freshening of Cl contents is stronger (see "Discussion," p. 8).

B isotopic compositions measured ($\delta^{11}B_{measured}$) were corrected for pH, temperature, and porosity changes after core recovery (for details, see You et al., 1996) and are then presented also as $\delta^{11}B_{in\ situ}$ (see different symbols in Fig. F5). The subsurface samples of Site 1150 are characterized by slightly more negative $\delta^{11}B$ values than seawater (SW = 39.5‰) (Spivack and Edmond, 1987), which results from the release of ^{10}B during bacterial processes (as also reported in Brumsack and Zuleger, 1992; You et al., 1996). Values of $\delta^{11}B$ decrease (between 32.7‰ and 35.4‰) at rather shallow depth (100–500 mbsf). Such a shift to $\delta^{11}B$ values lower than seawater might be explained by B desorption from clay (Spivack et al., 1987) or ash alteration (Brumsack and Zuleger, 1992). Between 650 and 1100 mbsf, the $\delta^{11}B$ values become significantly higher, exceeding seawater $\delta^{11}B$ (up to 46.4‰) (see Fig. F5). This strong trend toward more positive isotopic signatures corresponds to high B concentrations (up to ~2000 µM; ~4.5-fold SW) (see Fig. F5). In the lowest part of the hole, $\delta^{11}B$ values drop again (as low as 31‰) (Deyhle and Kopf, 2002), coinciding with high B contents (3900 µM; ~9.3-fold SW). This general trend of decreasing $\delta^{11}B$ together with a steady enrichment of the B concentrations with depth likely reflects preferential desorption of ^{10}B during the release of B, due to compaction and increasing temperatures (see "Discussion," p. 8).

F5. B isotopes, p. 21.

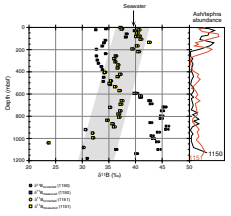

Site 1151

For Site 1151, Cl isotope data were not measured. B are presented in Figure F5 isotopes (see also Deyhle and Kopf, 2002). Generally, the surface samples are characterized by slightly lower $\delta^{11}B$ values than seawater (SW = 39.5‰), which results from the release of ^{10}B during bacterial processes (as also reported in Brumsack and Zuleger, 1992; You et al., 1996). Despite some scatter, the overall downhole $\delta^{11}B$ values decrease gradually. This general trend of decreasing $\delta^{11}B$ values (gray corridor in Fig. F5) together with a steady enrichment of B concentrations with depth (Fig. F3I) likely reflect preferential desorption of ^{10}B during the release of B, due to compaction and increasing temperatures (see discussion below).

Hydrocarbon Gases

F6. C_1/C_2 and C_2, p. 22.

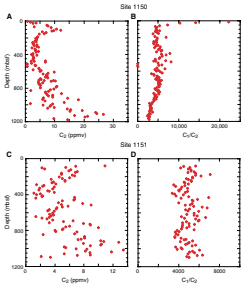

Site 1150

Headspace gas analyses indicate that methane (C_1) and ethane (C_2) are the only hydrocarbons above the detection limit. Methane concentrations range between 0.05% and 9%, whereas ethane abundance is relatively low (Fig. F6A). Although most data scatter between 0 and 10 parts per million volume (ppmv), there is a prominent increase to values as high as 26 ppmv in the lowermost part of the hole where frac-

tures are abundant. In fact, maximum values seem to coincide with the lower shear zone (1030–1070 mbsf) (see Fig. F6A). Free-gas samples extracted from the core liner reflect headspace results, with even higher C_2 values of 79–116 ppmv (Sacks, Suyehiro, Acton, et al., 2000). C_1/C_2 ratios also reflect this increase in ethane as indicated by a steady decrease from ~600 mbsf (~6000 ppmv) (Fig. F6B) to the base of the succession recovered (2500 ppmv) (Fig. F6B). Among possible explanations for our observations are hydrocarbon formation and upward migration of these gases through the fracture network and penetrative shear zones, microbial methanogenesis utilizing the abundant organic matter in the sediments, or gas hydrate dissociation (see "Discussion," p. 8).

Site 1151

Results from gas analyses are presented in Figure F6C and F6D. Methane is the dominant gas phase and does not change notably in the upper part of Site 1151 cores. Values in the shallow cores are ~4% and decrease to ~1%–2% between 300 and 400 mbsf (Sacks, Suyehiro, Acton, et al., 2000). The enrichment in the shallow part may be due to microbial production. Although no $\delta^{13}C$ data exist from these samples to corroborate this hypothesis, C_1/C_2 ratios >>1000, as seen at Site 1151 (as well as Site 1150), are generally interpreted as being typical of sedimentary environments with large methanogenic activity (Claypool and Kaplan, 1974). In the fractured interval (below 600 mbsf), methane values increase steadily to ~8%; however, a strong scatter is observed in these data. Ethane shows a similar downhole trend, with an increase from ~4 ppmv at 600 mbsf to ~13 ppmv at 1100 mbsf (Fig. F6C). In the lowermost 100 mbsf of the hole, a peculiar decrease back to 2 ppmv is seen. The same significant drop in methane concentrations to ~1% is observed. Owing to the similarity of the C_1 and C_2 concentrations as a function of depth, the C_1/C_2 ratio remains more or less constant over the entire succession. Data generally scatter from 4000 to 6000 ppmv (Fig. F6D). Consequently, the average C_1/C_2 ratio of the Site 1151 samples is higher than that at Site 1150, whereas the absolute C_2 concentrations are much lower. Methane concentrations are similar at the two drill sites (Sacks, Suyehiro, Acton, et al., 2000).

DISCUSSION

The discussion will focus on the origin of the fluids, their flow paths, and the possible causes for excursions of the pore water chemistry at Sites 1150 and 1151 and will be supplemented by the hydrocarbon data. As can be seen from the results presented by Sacks, Suyehiro, Acton, et al. (2000), Deyhle and Kopf (2002), and this manuscript, pore water chemistry shows strong anomalies from the expected downhole trends in the interval below ~600 mbsf. This depth range coincides with a considerable induration of the diatomaceous clays toward firm or even cemented claystone (Sacks, Suyehiro, Acton, et al., 2000). As a consequence, brittle failure of the sedimentary rocks is frequently observed, as indicated by the shaded areas in Figure F2. The main aspect to be addressed in the discussion is necessarily the origin(s) of the excursions in the pore fluid profiles. Possible candidate processes are in situ alteration reactions of the rocks in the deeper part of the borehole, external fluid influx from deeper levels utilizing the fractures and shear zones, or gas hydrate processes.

The most remarkable concentration changes in Sites 1150 and 1151 pore fluids are the low chlorinities, salinities, and alkalinities in the deep sediments below 600 mbsf (Figs. **F2A, F2B, F2G, F3A, F3B, F3G**). Possible processes contributing to such freshening may be clay mineral dehydration (Gieskes et al., 1990), alteration of biogenic silica (opal-quartz transformation) (Kastner, 1981), ash alteration (Gieskes and Lawrence, 1981), or gas hydrate dissociation (Kopf et al., 2000). Clay mineral dehydration may be caused by tectonic compaction (i.e., loss of interlayer water, as has been evidenced by Fitts and Brown, 1999) or may be a temperature-driven transformation of smectite to illite (e.g., Colten-Bradley, 1987). Similarly, biogenic silica (opal-A) may be transformed to secondary silica lepispheres and quartz, again mostly as a function of increasing temperature during burial (e.g., Moore and Gieskes, 1980). More locally, influx of meteoric waters through advection across porous sandstones and conglomerates has been previously put forward as an explanation for the low Cl contents (Moore and Gieskes, 1980). This latter finding, largely based on pore fluid chemistry of DSDP Sites 438 and 439 (adjacent to Site 1150), seems to be restricted to an area of ~1000 km^2 into which freshwater ceased to migrate prior to the major subsidence events in the Japan Trench forearc. Sacks, Suyehiro, Acton, et al. (2000) came to a similar conclusion, since ancient meteoric waters would have to originate from shallow-water deposits, which have not been recovered. Influx of fresh meteoric waters can equally be ruled out because the shoreline is >100 km away from the drilling locations (Sacks, Suyehiro, Acton, et al., 2000). Gas hydrate dissociation, which is a possibility since the drill sites are well within the stability zone of massive clathrates, has been shown to cause chlorinities in ODP pore waters to drop to one-half of SW concentration and below (Kopf et al., 2000). On the other hand, no bottom-simulating reflectors are observed in seismic reflection lines in the area (von Huene et al., 1994; Tsuru et al., 2000), which indicates that free gas is unlikely to be trapped beneath the hydrate stability zone. However, some concentrations of dissolved elements are extremely high (e.g., Li = ~40-fold SW concentration at Site 1150), so that we feel it is unlikely that this value was even higher in the original pore fluid prior to hydrate dissociation during core recovery. Even the measured values of Li or B are uncommon and among the highest measured in marine pore waters, suggesting that basically none of these soluble elements are taken up by the solid phases present.

Given the regional arguments against meteoric or hydrate waters as well as the SEM observations in the deep part of the Leg 186 drill sites, where diatom tests have been shown to be unaltered as well as physically intact (i.e., not crushed or collapsed) (S. Saito, pers. comm., 2001), we are left with either ash alteration and/or clay dehydration to explain the freshening.

In addition to chlorinity, decreasing element concentrations (like Mg, Na, and K) (Figs. **F2, F3**) (see Sacks, Suyehiro, Acton, et al., 2000) with depth may equally be explained by mineral dehydration–induced dilution but could also have been caused by preferential uptake of some elements during diagenetic reactions. Especially, the smectite to illite reaction may be a sink for elements like Mg or K (Perry and Hower, 1970). In addition, some of the pronounced enrichment patterns found in the interstitial waters (e.g., the strong B enrichment in the fractured interval of both sites) (Figs. **F2K, F3K**) could be a result of increasing tectonic stresses and temperatures, which cause the adsorbed B species to be released to the fluid (e.g., Spivack et al., 1987; You et al., 1993,

1996; Deyhle and Kopf, 2002). However, B may be mobilized during alteration of magmatic materials like tephra or basaltic crust as well (e.g., Palmer and Swihart, 1986), which would also result in a shift to more positive isotope ratios (as illustrated in Fig. F3B). Alteration of volcanic matter dispersed in the sedimentary column (both as patches and thin beds), furthermore, appears to have a profound effect on dissolved constituents in the pore water. Namely, mobile elements like B, Sr, and Li are affected, resulting in pronounced enrichments of the latter element (e.g., ~440 µM in the fractured interval of Site 1150) (Fig. F2H). Although there are distinct periods of enhanced volcanism (especially during the most recent Earth history), the increase of most elements is linear and does not show maxima in the fractured interval where volcanic matter is most abundant (i.e., at the base of Site 1150) (see Fig. F1B, right column). This would be in agreement with the observation that the majority of the ash and tephra layers appear unaffected or only slightly altered (Y. Najman, pers. comm., 2001). On the other hand, the strong deviation of Ca vs. Mg contents from a linear relationship (Fig. F7) may be taken as indirect evidence for alteration of magmatic material (see McDuff, 1978, 1981) and at Sites 1150 and 1151 is in fact more accentuated than similar data from other drill sites (see compilation in Gieskes and Lawrence, 1981).

F7. Ca vs. Mg, p. 23.

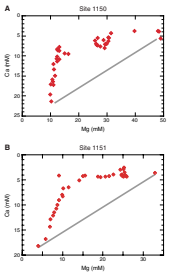

Two competing hypotheses can explain the observed patterns at Leg 186 sites: in situ alteration of fluids or upward migration of a fluid already altered at depth. In situ alteration is unlikely to have had a profound effect on the clays and diatoms in the Leg 186 sediments. In Miocene sediments similar to those from Leg 186, Murata et al. (1977) found that a temperature window of 41°–56°C is required to significantly alter opal-A. For these reasons, both smectite-illite reactions and silica diagenesis are unlikely to have profound effects in the ~1200 m drilled at Sites 1150 and 1151 because in this part of the Japan Trench forearc the geothermal gradient is ~30°–35°C/km (Sacks, Suyehiro, Acton, et al., 2000). Also, Moore and Gieskes found only very minor formation of secondary silica lepispheres from diatom tests at ~850 mbsf at DSDP Site 438 (temperature = 31°C) and Saneatsu Saito (pers. comm., 2001) observed largely intact diatom tests in deep sediment samples from Leg 186 using SEM. As it has been shown in hydrothermal experiments by Kastner et al. (1977), silica diagenesis is retarded during clay alteration because smectite is a competitor for Mg^{2+} and OH^- ions required for opal-A/opal-CT transformation. Silica diagenesis can also be ruled out given that B contents increase with depth (Figs. F2K, F3K), whereas a significant decrease in B has been reported from ODP Sites 794–797 in the Japan Sea below the opal-A/opal-CT transition (Brumsack and Zuleger, 1992). The latter is most likely a result of water being released from the amorphous tests during the transformation reaction. As for clay mineral processes, smectite contents are generally high (often ~50%–70% of the clay portion) (Ask and Kopf, in press), which further rules out in situ transformation to illite. All the abovementioned alteration processes may well play a role below the terminal depths of the Leg 186 sites, so that deep fluids affected by them could well have been picked up in the fractured rocks recovered.

The two competing mechanisms explaining the isotope excursions and the element enrichment/depletion patterns in the studied fluids are ash alteration and deep-seated processes (clay transformation, etc.). As can be seen from Figure F1, there is an increase in volcanic activity in the upper Miocene. However, this increase affects mostly the lowermost part of the boreholes below 1000 mbsf. It therefore may account

for the strongest Sr, Li, and B enrichments (Figs. F2F, F2H, F2K, F3F, F3H, F3K, respectively) and decrease in $\delta^{11}B$ values (Fig. F5) near the base of the two holes and may equally be responsible for an increase in Cl at the very bottom of Site 1150 (Martin, 1999). It is, however, unlikely to be the reason for the overall deviation of the downhole trends from ~600 to 1200 mbsf (Figs. F2, F3) (Sacks, Suyehiro, Acton, et al., 2000). For instance, the strong depletion of Li (Fig. F3H) at Site 1151 would be in conflict with alteration of ash in these Miocene sediments.

By contrast, the deep fluid hypothesis is supported by several arguments. First, fluid pathways exist in the firm claystones in the deeper part of Sites 1150 and 1151, represented by a several hundred-meter-thick fractured interval at either site as well as two shear zones at 900–950 and 1030–1070 mbsf at Site 1150. Second, illitization of smectite is believed to begin at ~60°–70°C and to finish at ~120°–150°C (e.g., Colten-Bradley, 1987). Given the thermal gradient of ~30°–35°C/km, temperatures sufficient for clay diagenesis and similar temperature-driven processes should occur well below the terminal depth of the drill hole. Based on the continuously strong downhole increase of B and Li and decrease in Cl, we conclude that the majority of the pore fluid signatures are affected by clay mineral water release and simultaneous cation desorption from transforming claystones, due to incipient pressure and temperature with depth. Such a trend has previously been described for other forearcs (e.g., You et al., 1993, 1995; Deyhle and Kopf, 2002). At permeable faults, such as the décollements of the Nankai accretionary prism farther south (~3000 µM B; i.e., 7-fold SW) and the Barbados Ridge (~1500 µM B; i.e., 3.5-fold SW) (You et al. 1993), deep-seated fluids migrate to shallow depth. B concentration is highest where faults intersect the drilled profiles, which have been interpreted as normal-sense shear zones at the base of Site 1150 (Sacks, Suyehiro, Acton, et al., 2000). The fluids migrating through these shear zones have even higher B concentrations and isotope values (Figs. F2K, F5). Similarly, $\delta^{37}Cl$ values of the deep-seated shear zone fluids have very distinct signatures (Fig. F4), supporting an external fluid influx into the deeper portion of Site 1150. This migration of fluids does not produce a strong discontinuity in the downhole pore water profile, which is suggestive that flow may be episodic. On the other hand, only some décollements show abrupt deviations of pore water curves (Nankai and Barbados) (You et al., 1993), whereas others show a minor discontinuity (Costa Rica) (Kopf et al., 2000).

The interpretation based on $\delta^{11}B$ data is not as straightforward as it is for B contents between the two drill sites. Because clays preferentially contain ^{10}B, desorption at depth is expected to produce lower $\delta^{11}B$ values than seawater (and to have higher B contents, as indicated by the gray corridor in Fig. F5). This observation is in agreement with the B concentrations and the isotope data of Leg 186 pore waters (Figs. F2K, F3K); however, it fails to explain the shift to lower $\delta^{11}B$ values between 100 and 400 mbsf and the positive shift to higher $\delta^{11}B$ values between 600 and 1100 mbsf at Site 1150 (Fig. F5). In the fractured and sheared depth intervals of Site 1150, B contents reach maxima of almost 10-fold SW concentration and $\delta^{11}B$ values are high (Fig. F5). Such elevated $\delta^{11}B$ values can be related to preferential uptake of ^{10}B into mineral lattices, such as illite (e.g., Williams et al., 2001) or tourmaline minerals (Palmer and Swihart, 1996). Hence, out-of-sequence faults in the Cretaceous margin wedge and overlying, hydraulically connected normal shear zones in the slope apron do both favor to some extent the backflux of

geochemically mature fluids from the foreac into the ocean. Such fluid flux (and expulsion in the forearc) is indirectly supported from geochemical studies of the northeast Japan arc lavas, which attest that the contribution of sediment-derived fluid into magma genesis is only 10% (Sano et al., 2001). Consequently, most of the fluid from the underthrust sequence and the forearc wedge migrates upward along the décollement, out-of-sequence thrusts, and shear zones (as drilled during Leg 186) into the ocean.

If we compare the depth trends of the different constituents in the pore fluids of either drill site there are general similarities, but there is also one distinctive pattern in the interval between ~200 and 600 mbsf at Site 1150. Good agreement exists between the profiles of alkalinity (Figs. **F2F, F3F**), ammonium (Sacks, Suyehiro, Acton, et al., 2000), sulfate, and boron (Figs. **F2K, F3K**). However, compared to the overall downhole trends (no matter whether increasing or decreasing), the interval from 200 to 600 mbsf shows excursions in many of the other elements. Salinity, Cl, K, Na, Mg, Li, and Sr increase relative to the expected downhole trend (Figs. **F2, F3**). Also, Cl isotope values increase (Fig. **F4**). The combined evidence of these excursions can best be explained by the release of a fluid of seawater-like composition, as has been argued previously based on evidence from a comprehensive B geochemical study (see discussion in Deyhle and Kopf, 2002).

The results drawn from pore water studies are supported by the gas data (Fig. **F6**). Whereas methane concentrations are similar at the two drill sites (Sacks, Suyehiro, Acton, et al., 2000), there is a more profound enrichment in C_2 concentrations at Site 1150. Since not only C_1/C_2 decreases, but absolute C_2 concentrations increase, methanogenesis alone cannot explain the data. Gas hydrate dissociation has also been ruled out for other reasons (see above). The high C_2 content at Site 1150 is probably a result of conductive discharge of fluids rich in deep-seated gas along shear zones and fracture networks, especially when compared to Site 1151, where no major shear zones were penetrated. This contention is supported by the fact that average C_1/C_2 ratios of the Site 1151 gas samples are higher than those at Site 1150, whereas the absolute C_2 concentrations are much lower. However, both sites show lowest values (i.e., strongest thermal maturation signal) well above 1000 ppmv, which has been accepted as the lower boundary of the field of microbial methane production in the sediment (Claypool and Kaplan, 1974). Consequently, we conclude that most of the gas sampled from Leg 186 drill cores originates from shallow to moderate depth within the Japan Trench forearc.

CONCLUSIONS

The results from the geochemical study of ODP Leg 186 pore fluid and gas samples can be summarized to the following conclusions:

1. The prominent excursion of the majority of the element concentration profiles and isotope curves with depth suggest that a deep-seated fluid migrates into the lower half (~600–1200 mbsf) of the sedimentary succession drilled at Sites 1150 and 1151, Japan Trench forearc. Main processes operating at depth are clay mineral transformation (causing freshening of the pore fluid), desorption reactions (causing enrichment in B and other ele-

ments), and—to a lesser extent—formation of secondary silica from opal-A.

2. Chlorinity and salinity of pore waters from the two sites drilled during Leg 186 are much lower than those reported from deep-seated décollement zones at Nankai, Barbados, and so on. This freshening attests to mobilization of mineral water at depth, which is then expelled along permeable faults and shear zones.
3. Deep-seated processes in the fractured intervals of Sites 1150 and 1151 are further shown by elevated hydrocarbon contents and decrease of the C_1/C_2 ratios (especially at Site 1150) in gas samples from both drill sites.
4. In situ alteration of ash and tephra may account for some excursion of the pore fluid profiles (e.g., Sr and Sr isotopes), especially in the deeper part of Site 1150. This result is supported by other observations such as the strongly nonlinear Ca/Mg relationship.
5. Extremely enriched concentrations of B (almost 10-fold SW concentration), Sr, but also Ca and Li are observed in the Leg 186 pore waters, although salinities and chlorinities of the same fluids drop to nearly one-half the seawater concentration. Compared to fluids from the décollement zones of accretionary prisms, an even stronger B enrichment occurs in these fluids from shear zones in the upper slope of the Japan Trench forearc. Thus, the B backflux from sediments into the ocean might have been underestimated previously (see Kopf et al., 2001) when B geochemical mass balances focused mostly on fluids venting from décollements of accretionary prisms. Although less pronounced, the same effect is observed for other elements.

ACKNOWLEDGMENTS

We thank Lorraine Albrecht (mass spectrometry; Waterloo), Regina Surberg (ICP-AES; Kiel), and Dieter Garbe-Schönberg (ICP-MS; Kiel) for help with the analyses and the Shipboard Scientific Party of ODP Leg 186 for discussion. The manuscript benefitted from suggestions and criticisms by Jon Martin and Jeff Ryan, for which we are most grateful. This research used samples and data provided by the Ocean Drilling Program (ODP). The ODP is sponsored by the U.S. National Science Foundation (NSF) and participating countries under management of Joint Oceanographic Institutions (JOI), Inc. Funding for this research was provided by the Alexander-von-Humboldt Stiftung (to A.K.) and DAAD (Deutscher Akademischer Austauchdienst) and DFG (Deutsche Forschungsgemeinschaft; DE 819/1-1) fellowships (to A.D.).

REFERENCES

Ask, M.V.S., and Kopf, A., in press. Rock mechanic characteristics of ODP Leg 186 claystones in the Japan Trench forearc, and their relationship to lithology, geologic structures, physical properties and seismicity. *Isl. Arc*.

Brumsack, H.-J., and Zuleger, E., 1992. Boron and boron isotopes in pore waters from ODP Leg 127, Sea of Japan. *Earth Planet. Sci. Lett.,* 113:427–433.

Cadet, J.-P., Kobayashi, K., Aubouin, J., Boulège, J., Dubois, J., von Huene, R., Jolivet, L., Kanazawa, T., Kasahara, J., Koizumi, K., Lallemand, S., Nakamura, Y., Pautout, G., Suyehiro, K., Tani, S., Tokuyama, H., and Yamazaki, T., 1985. De la fosse du Japon à la fosse des Kouriles: premier résultats de la campagne océanographique franco-japonaise Kaiko (Leg III) *C. R. Acad. Sci. Paris, Sér. II, Mec., Phys., Chim., Sci. Terre, Univers,* 301:287–296.

Claypool, G.E., and Kaplan, I.R., 1974. The origin and distribution of methane in marine sediments. *In* Kaplan, I.R. (Ed.), *Natural Gases in Marine Sediments:* New York (Plenum), 99–139.

Colten-Bradley, V.A., 1987. Role of pressure in smectite dehydration—effects on geopressure and smectite-to-illite transformation. *AAPG Bull.,* 71:1414–1427.

Deyhle, A., and Kopf, A., 2002. Strong B-enrichment and anomalous boron isotope geochemistry in the Japan forearc. *Mar. Geology,* 183:1–15.

Fitts, T., and Brown, K., 1999. Stress-induced smectite dehydration: ramifications for patterns of freshening and fluid expulsion in the N. Barbados accretionary wedge. *Earth Planet. Sci. Lett.,* 172:179–197

Gieskes, J.M., Blanc, G., Vrolijk, P., Elderfield, H., and Barnes, R., 1990. Interstitial water chemistry—major constituents. *In* Moore, J.C., Mascle, A., et al., *Proc. ODP, Sci. Results,* 110: College Station, TX (Ocean Drilling Program), 155–178.

Gieskes, J.M., and Lawrence, J.R., 1981. Alteration of volcanic matter in deep-sea sediments: evidence from the chemical composition of interstitial waters from deep sea drilling cores. *Geochim. Cosmochim. Acta,* 45:1687–1703.

Harder, H., 1973. Boron. *In* Wedepohl, K.H. (Ed.), *Handbook of Geochemistry II-1:* Berlin (Springer).

Hawkesworth, C.J., and Elderfield, H., 1978. The strontium isotopic composition of interstitial waters from Sites 245 and 336 of the Deep Sea Drilling Project. *Earth Planet. Sci. Lett.,* 40:423–432.

Kagami, H., Karig, D.E., Coulbourn, W.T., et al., 1986. *Init. Repts. DSDP,* 87: Washington (U.S. Govt. Printing Office).

Kastner, M., 1981. Authigenic silicates in deep sea sediments: formation and diagenesis. *In* Emiliani, C. (Ed.), *The Sea* (Vol. 7): *The Oceanic Lithosphere:* New York (Wiley), 915–980.

Kastner, M., Keene, J.B., and Gieskes, J.M., 1977. Diagenesis of siliceous oozes, I. Chemical controls on the rate of opal-A to opal-CT transformation—an experimental study. *Geochim. Cosmochim. Acta,* 41:1041–1059.

Kastner, M., and Spivack, A.J., 2001. New insights on the fluid flow regime in the Nankai Trough subduction zone. *Eos Trans. Am. Geophys. Union,* 82:F1247–1248.

Kaufmann, R.S., 1984. Chlorine in groundwater: stable isotope distribution [Ph.D. dissert.]. Univ. of Arizona, Phoenix.

Kopf, A., Deyhle, A., Zuleger, E., 2000. Evidence for deep fluid circulation and gas hydrate dissociation using boron isotopes of pore fluids in forearc sediments from Costa Rica (ODP Leg 170). *Mar. Geol.,* 167:1–28.

Kvenvolden, K.A., and McDonald, T.J., 1986. Organic geochemistry on the *JOIDES Resolution*—an assay. *ODP Tech. Note,* 6.

Langseth, M.G., von Huene, R., Nasu, N., and Okada, H., 1981. Subsidence of the Japan Trench forearc region of northern Honshu. In *Colloquium C3: Geology of Continental Margins: 26th International Geological Congress*. Oceanol. Acta, 4:173–179.

Martin, J.B., 1999. Nonconservative behavior of Br^-/Cl^- ratios during alteration of volcaniclastic sediments. *Geochim. Cosmochim. Acta,* 63:383–391.

McDuff, R.E., 1978. Conservation behavior of calcium and magnesium in interstitial waters of marine sediments: identification and interpretation [Ph.D. dissert.]. Univ. of California, San Diego.

————, 1981. Major cation gradients in DSDP interstitial waters: the role of diffusive exchange between seawater and upper oceanic crust. *Geochim. Cosmochim. Acta,* 45:1705–1713.

Moore, G.W., and Gieskes, J.M., 1980. Interactions between sediment and interstitial water near the Japan Trench, Leg 57, Deep Sea Drilling Project. *In* von Huene, R., Nasu, N., et al., *Init. Repts. DSDP,* 56, 57 (Pt. 2): Washington (U.S. Govt. Printing Office), 1269–1275.

Murata, K.J., Friedman, I., and Gleason, J.D., 1977. Oxygen isotope relations between diagenetic silica minerals in Monterey Shale, Temblor Range, California. *Am. J. Sci.,* 277:259–272.

Nasu, N., von Huene, R., Ishiwada, Y., Langseth, M., Bruns, T., and Honza, E., 1980. Interpretation of multichannel seismic reflection data, Legs 56 and 57, Japan Trench transect, Deep Sea Drilling Project. *In* Scientific Party, *Init. Repts. DSDP,* 56, 57 (Part 1): Washington (U.S. Govt. Printing Office), 489–503.

Palmer M.P., and Swihart, G.H., 1996. Boron isotope geochemistry: an overview. *In Boron Mineralogy, Petrology, and Geochemistry.* Mineral. Soc. Am., Rev. Mineral., 33:709–744.

Perry, E., and Hower, J., 1970. Burial diagenesis in Gulf Coast pelitic sediments. *Clays Clay Miner.,* 18:165–177.

Sacks, I.S., Suyehiro, K., Acton, G.D., et al., 2000. *Proc. ODP, Init. Repts.,* 186 [CD-ROM]. Available from: Ocean Drilling Program, Texas A&M University, College Station TX 77845-9547, USA.

Sano, T., Hasenaka, T., Shimaoka, A., Yonezawa, C., and Fukuoka, T., 2001. Boron contents of Japan Trench sediments and Iwate basaltic lavas, northeast Japan arc: estimation of sediment-derived fluid contribution in mantle wedge. *Earth Planet. Sci. Lett.,* 186:187–198.

Sayles, F.L., and Manheim, F., 1975. Interstitial solutions and diagenesis in deeply buried marine sediments: results from the Deep Sea Drilling Project. *Geochim. Cosmochim. Acta,* 39:103–127.

Scientific Party, 1980a, *Init. Repts. DSDP,* 56, 57 (Pt. I): Washington (U.S. Govt. Printing Office), 1–629.

————, 1980b. *Init. Repts. DSDP,* 56, 57 (Pt. II): Washington (U.S. Govt. Printing Office), 633–1417.

Shipboard Scientific Party, 2000. Explanatory notes. *In* Sacks, I.S., Suyehiro, K., Acton, G.D., et al., *Proc. ODP, Init. Repts.,* 186, 1–51 [CD-ROM]. Available from: Ocean Drilling Program, Texas A&M University, College Station TX 77845-9547, USA.

Sie, P.M.J., and Frape, S.K., 2002. Evaluation of the groundwaters from the Stripa mine using stable chlorine isotopes. *Chem. Geol.,* 182:565–582.

Spivack, A.J., and Edmond, J.M., 1987. Boron isotope exchange between seawater and oceanic cust. *Geochim. Cosmochim. Acta,* 51:1033–1043.

Spivack, A.J., Palmer, M.R., and Edmond, J.M., 1987. The sedimentary cycle of the boron isotopes. *Geochim. Cosmochim. Acta,* 51:1939–1949.

Suyehiro, K., and Nishizawa, A., 1994. Crustal structure and seismicity beneath the forearc off northeastern Japan. *J. Geophys. Res.,* 99:22331–22348.

Tsuru, T., Park, J.-O., Takahashi, N., Kochira, S., Kido, Y., Kaneda, Y., and Kono, Y., 2000. Tectonic features of the Japan Trench convergent margin off Sanriku, northeastern Japan, revealed by multichannel seismic reflection data. *J. Geophys. Res.,* 105:16403–16413.

von Huene, R., and Culotta, R., 1989. Tectonic erosion at the front of the Japan Trench convergent margin. *Tectonophysics,* 160:75–90.

von Huene, R., Klaeschen, D., Cropp, B., and Miller, J., 1994. Tectonic structure across the accretionary and erosional parts of the Japan Trench margin. *J. Geophys. Res.,* 99:22349–22361.

von Huene, R., and Lallemand, S., 1990. Tectonic erosion along the Japan and Peru convergent margins. *Geol. Soc. Am. Bull.,* 102:704–720.

von Huene, R., Langseth, M., Nasu, N., and Okada, H., 1982. A summary of Cenozoic tectonic history along IPOD Japan Trench transect. *Geol. Soc. Am. Bull.,* 93:829–846.

Williams, L.B., Hervig, R.L., Holloway, J.R, and Hutcheon, I., 2001. Boron isotope geochemistry during diagenesis, Part I. Experimental determination of fractionation during illitization of smectite. *Geochim. Cosmochim. Acta,* 65:1769–1782.

You, C.-F., Chan, L.H., Spivack, A.J., and Gieskes, J.M., 1995. Lithium, boron, and their isotopes in sediments and pore waters of Ocean Drilling Program Site 808, Nankai Trough: implications for fluid expulsion in accretionary prisms. *Geology,* 23:37–40.

You, C.-F., Spivack, A.J., Gieskes, J.M., Martin, J.B., and Davisson, M.L., 1996. Boron contents and isotopic compositions in pore waters: a new approach to determine temperature induced artifacts-geochemical implications. *Mar. Geol.,* 129:351–361.

You, C.-F., Spivack, A.J., Smith, J.H., and Gieskes, J.M., 1993. Mobilization of boron at convergent magins: implications for boron geochemical cycle. *Geology,* 21:207–210.

Zuleger, E., and Erzinger, J., 1991. Determination of boron isotopes using negative thermal ionization mass spectrometry. *Finnigan Isotope Mass Spectromet. Appl. Rept.*, 78.

Figure F1. Simplified (**A**) Site 1150 and (**B**) Site 1151 drilling information, including major lithologies, degree of sediment induration, sediment accumulation rates, and ash abundance (compiled from Sacks, Suyehiro, Acton, et al., 2000).

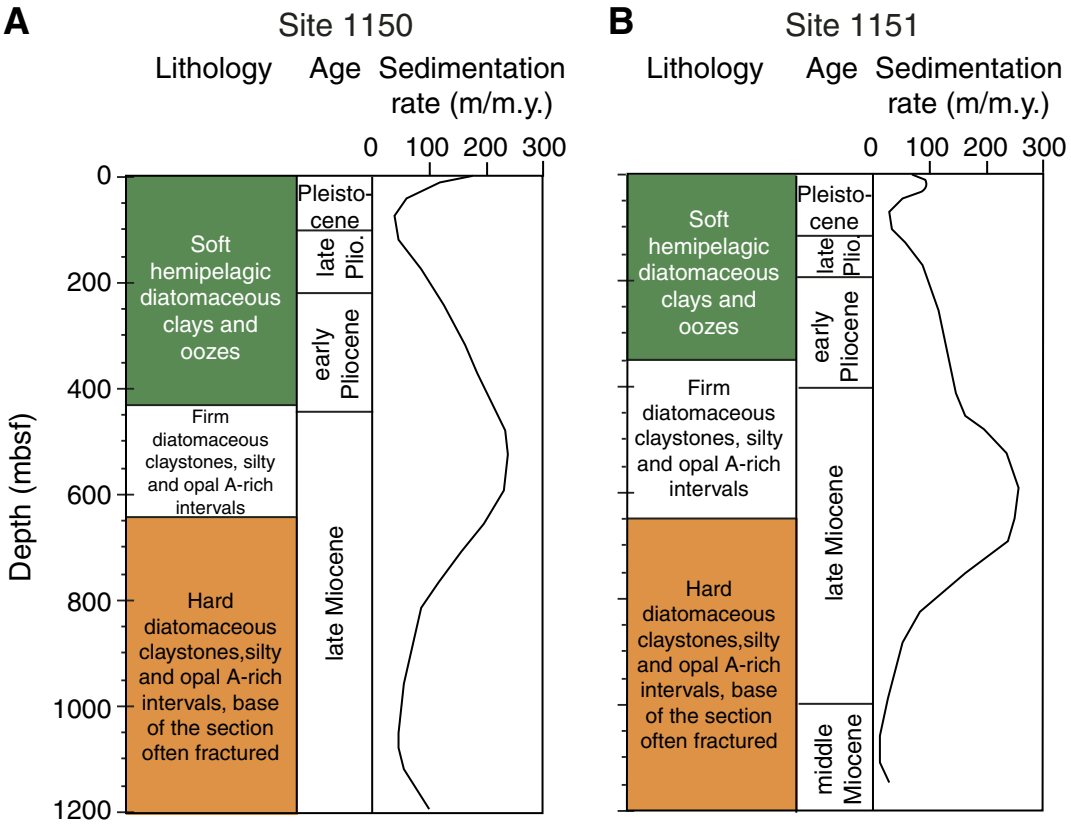

Figure F2. Pore water concentrations of (**A**) Cl, (**B**) salinity, (**C**) Na, (**D**) Mg, (**E**) K, (**F**) alkalinity, (**G**) Sr, (**H**) Li, (**I**) Ca, and (**K**) B vs. depth at Site 1150. Shaded intervals are zones with abundant faults and fractures; dark shading = shear zones.

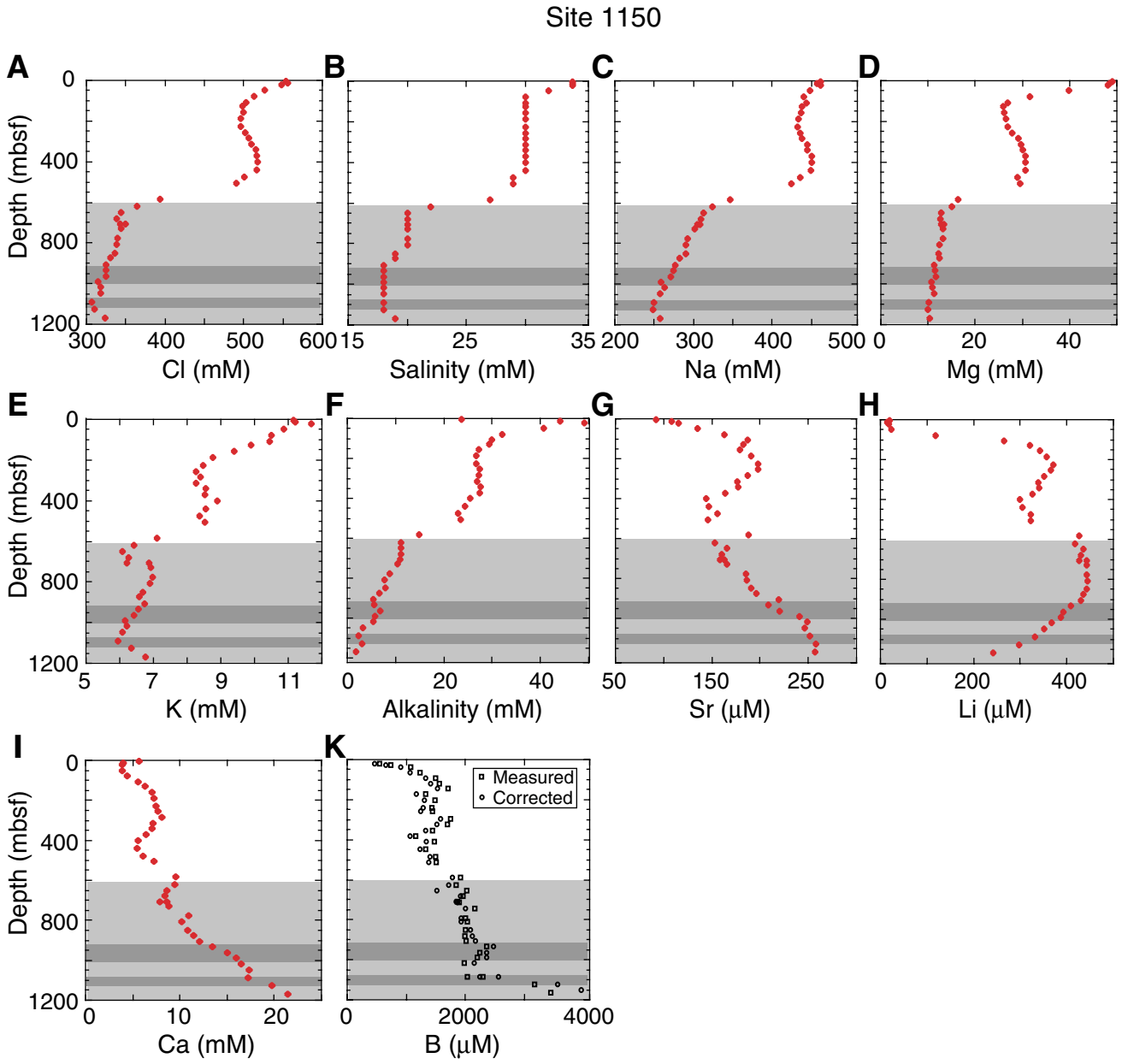

Figure F3. Pore water concentrations of (**A**) Cl, (**B**) salinity, (**C**) Na, (**D**) Mg, (**E**) K, (**F**) alkalinity, (**G**) Sr, (**H**) Li, (**I**) Ca, and (**K**) B vs. depth at Site 1151. Shaded intervals are zones with abundant faults and fractures.

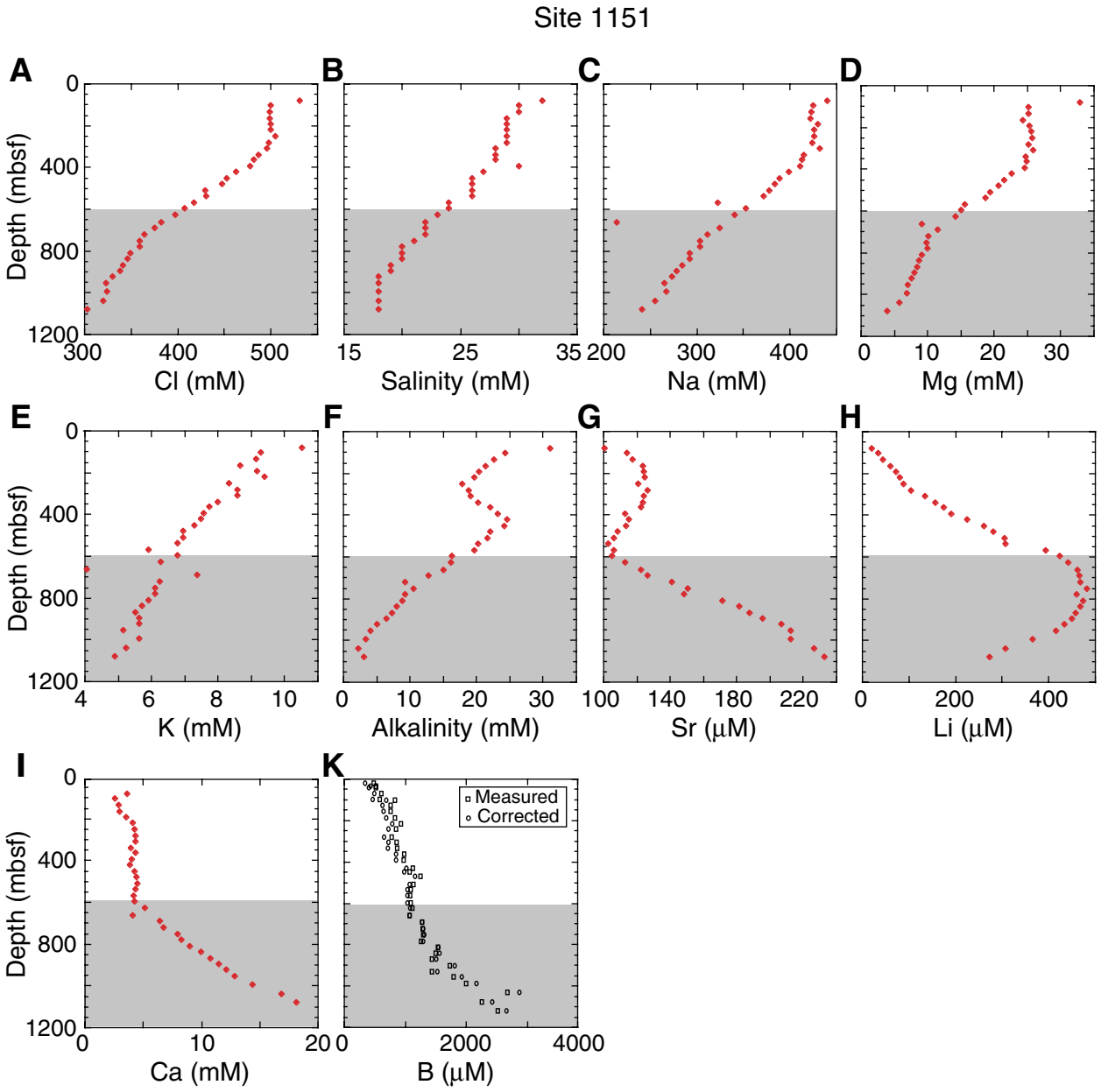

Figure F4. Cl isotope signatures vs. depth from pore fluids at Site 1150.

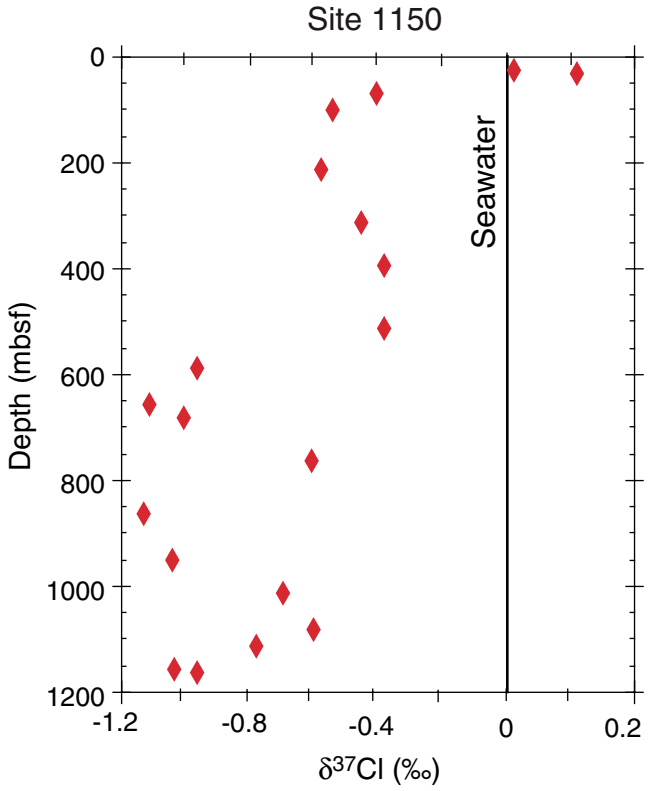

Figure F5. B isotope signatures of pore fluids at Sites 1150 and 1151. Note that B isotopic compositions measured were corrected for pH, temperature, and porosity changes after core recovery (for details, see You et al., 1996). The $\delta^{11}B_{corrected}$ values (assumed to represent $\delta^{11}B_{in\ situ}$) show only a small deviation from $\delta^{11}B_{measured}$, typically resulting in negligible shifts that lie within the analytical error of the thermal ion mass spectrometry analyses. The gray corridor represents the anticipated fractionation trend with depth. Right depth trends reflect relative ash abundance in sediments from Sites 1150 and 1151.

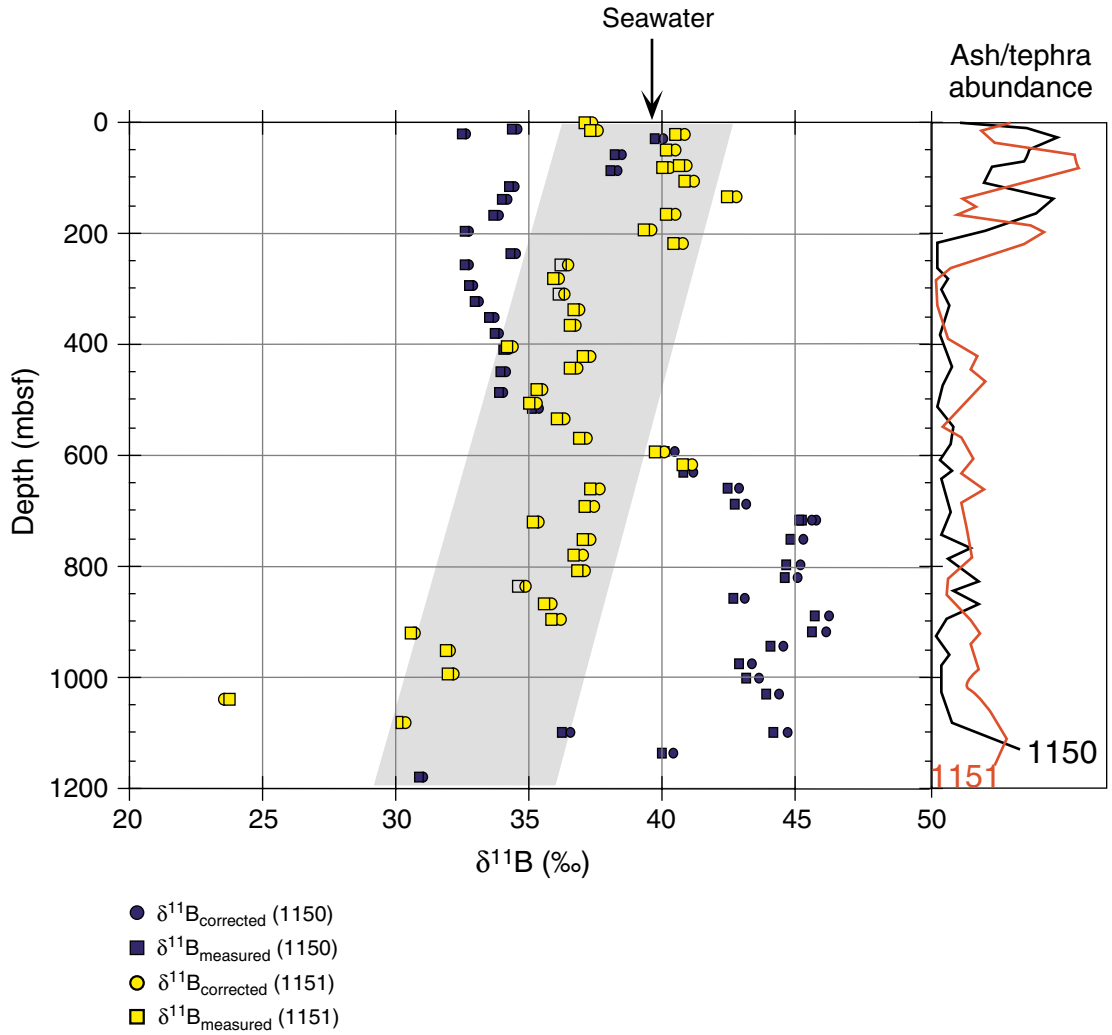

Figure F6. C_1/C_2 ratio and C_2 contents of gas samples recovered from (**A**, **B**) Site 1150 and (**C**, **D**) Site 1151.

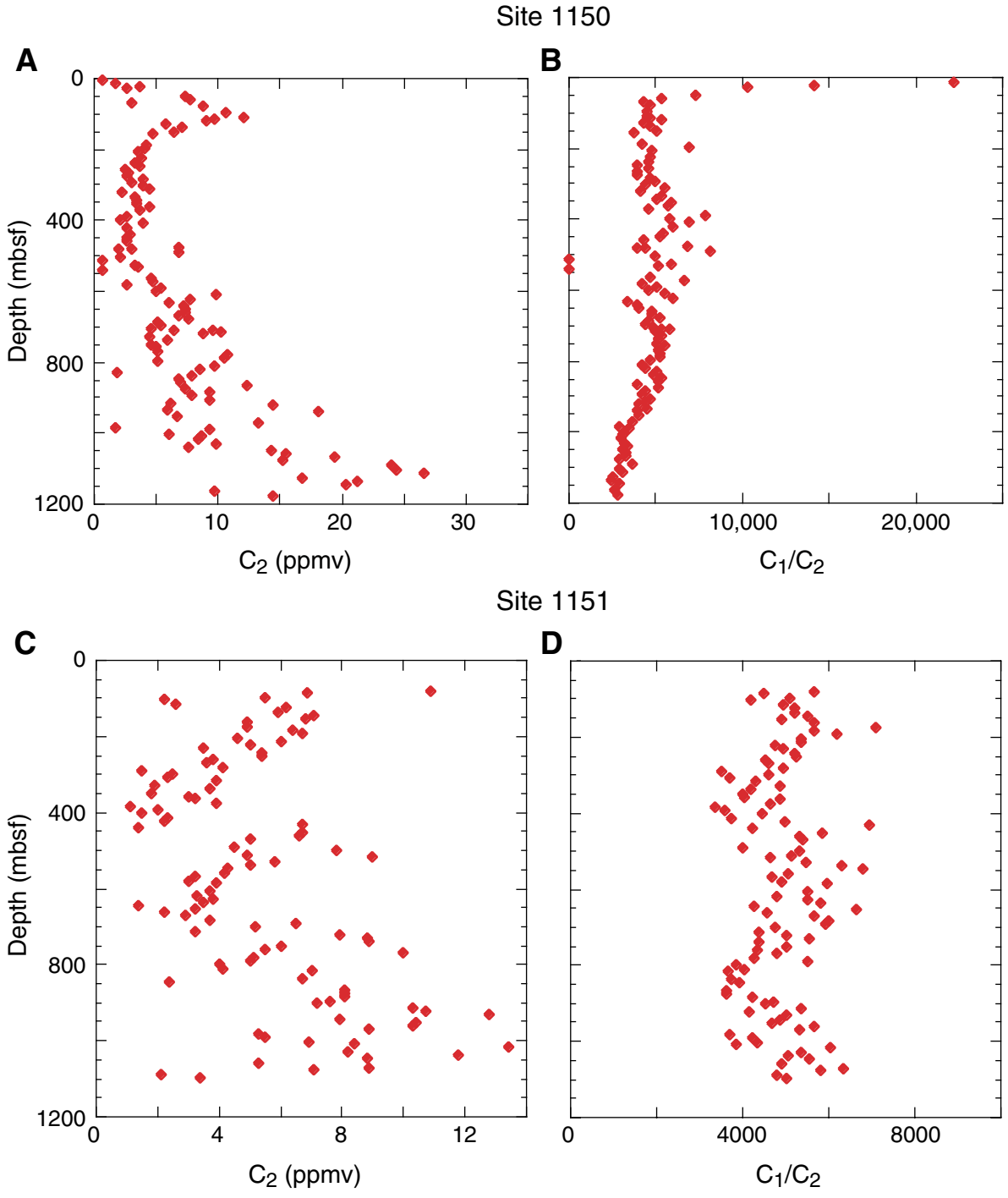

Figure F7. Ca vs. Mg contents in pore fluids from (**A**) Site 1150 and (**B**) Site 1151. Diagonal lines are placed to help illustrate the strong deviation of the data. Note that deviations are more pronounced than at any DSDP site studied by Gieskes and Lawrence (1981).